Human nonsense-mediated mRNA decay factor UPF2 interacts directly with eRF3 and the SURF complex

AUTHOR(S):

López-Perrote, Andrés; Castaño, Raquel; Melero, Roberto; Zamarro, Teresa; Kurosawa, Hitomi; Ohnishi, Tetsuo; Uchiyama, Akiko; ... Kataoka, Naoyuki; Yamashita, Akio; Llorca, Oscar

CITATION:

López-Perrote, Andrés ...[et al]. Human nonsense-mediated mRNA decay factor UPF2 interacts directly with eRF3 and the SURF complex. Nucleic Acids Research 2016, 44(4): 1909-1923

ISSUE DATE:

2016-02-29

URL:

http://hdl.handle.net/2433/216281

Published online 5 January 2016

Nucleic Acids Research, 2016, Vol. 44, No. 4 ***1909–1923***
doi: 10.1093/nar/gkv1527

Human nonsense-mediated mRNA decay factor UPF2 interacts directly with eRF3 and the SURF complex

Andrés López-Perrote[1,†], Raquel Castaño[1,†], Roberto Melero[1,†], Teresa Zamarro[1], Hitomi Kurosawa[2], Tetsuo Ohnishi[2], Akiko Uchiyama[2], Kyoko Aoyagi[2], Gretel Buchwald[3], Naoyuki Kataoka[4], Akio Yamashita[2,*] and Oscar Llorca[1,*]

[1]Centro de Investigaciones Biológicas, Consejo Superior de Investigaciones Científicas (Spanish National Research Council), Ramiro de Maeztu 9, 28040 Madrid, Spain, [2]Department of Molecular Biology, Yokohama City University School of Medicine, 3–9, Fukuura, Kanazawa-ku, Yokohama, Kanagawa 236-0004, Japan, [3]Max Planck Institute of Biochemistry, Department of Structural Cell Biology, Am Klopferspitz 18, D-82152 Martinsried, Germany and [4]Medical Innovation Center, Laboratory for Malignancy Control Research, Kyoto University Graduate School of Medicine, 53, Shogoin Kawaharacho, Sakyo-ku, Kyoto 606-8507, Japan

Received July 20, 2015; Revised December 11, 2015; Accepted December 22, 2015

ABSTRACT

Nonsense-mediated mRNA decay (NMD) is an mRNA degradation pathway that regulates gene expression and mRNA quality. A complex network of macromolecular interactions regulates NMD initiation, which is only partially understood. According to prevailing models, NMD begins by the assembly of the SURF (SMG1–UPF1–eRF1–eRF3) complex at the ribosome, followed by UPF1 activation by additional factors such as UPF2 and UPF3. Elucidating the interactions between NMD factors is essential to comprehend NMD, and here we demonstrate biochemically and structurally the interaction between human UPF2 and eukaryotic release factor 3 (eRF3). In addition, we find that UPF2 associates with SURF and ribosomes in cells, in an UPF3-independent manner. Binding assays using a collection of UPF2 truncated variants reveal that eRF3 binds to the C-terminal part of UPF2. This region of UPF2 is partially coincident with the UPF3-binding site as revealed by electron microscopy of the UPF2–eRF3 complex. Accordingly, we find that the interaction of UPF2 with UPF3b interferes with the assembly of the UPF2–eRF3 complex, and that UPF2 binds UPF3b more strongly than eRF3. Together, our results highlight the role of UPF2 as a platform for the transient interactions of several NMD factors, including several components of SURF.

INTRODUCTION

Nonsense mediate mRNA decay (NMD) was originally described as a quality control pathway whose function was to identify mRNAs containing premature termination codons (PTCs), which were then targeted for degradation (1–3). Such mRNAs could generate truncated proteins that can be non-functional and/or affect normal cellular functions by dominant-negative effects (4). NMD also plays a broader role as one of several core cellular mechanisms that regulate gene expression of a significant number of physiological mRNAs (5,6). Interestingly, recent evidence revealed that NMD is important for stem cell differentiation by regulating the decay of mRNAs encoding factors essential for differentiation and development of the embryo (7,8).

Deciding if an mRNA will be targeted for degradation by the NMD pathway is defined during translation. Several factors that bind to the translating ribosome and additional cis- and trans-acting factors are required for NMD initiation (3). These factors interact to assemble a complex set of transient macromolecular complexes. Describing and characterizing the interactions between all NMD factors, as well as the similarities and differences between species, is essential to understand how an NMD response is triggered and regulated. In mammals, three UPF (UP-Frameshift) proteins conserved in eukaryotes, UPF1, an ATP-dependent RNA helicase, UPF2 and UPF3, as well as the SMG1 (Suppressor with Morphogenetic effect on Genitalia 1) kinase complex (SMG1C), consisting of SMG1, SMG8 and SMG9, comprise the core NMD machinery (2,3). In mam-

*To whom correspondence should be addressed. Tel: +34 91 837 3112 (Ext 4446); Fax: +34 91 536 0432; Email: ollorca@cib.csic.es
Correspondence may also be addressed to Dr Akio Yamashita. Tel: +81 45 787 2598; Fax: +81 45 785 4140; Email: yamasita@yokohama-cu.ac.jp
†These authors contributed equally to the paper as first authors.
Present addresses:
Roberto Melero, Centro Nacionional de Biotecnología (CNB), Consejo Superior de Investigaciones Científicas (Spanish National Research Council, CSIC); Darwin 3, 28049 Madrid, Spain.
Tetsuo Ohnishi, Laboratory for Molecular Psychiatry, Brain Science Institute, RIKEN, Wako 351-0198, Japan.

mals, UPF3 appears in two variants, UPF3a and UPF3b, and we focus on UPF3b in this work (2).

A prevailing model suggests that UPF1 is recruited to stalled ribosomes as part of the SURF (SMG1–UPF1-eRF1–eRF3) complex, containing UPF1 helicase, SMG1 kinase and the eukaryotic release factors eRF1 (49 kDa) and eRF3 (69 kDa) that control translation termination in eukaryotes (3,9,10). UPF1 also binds mRNAs quite promiscuously and independently of translation, whereas translation has been shown to affect the distribution of UPF1 on mRNAs (11–13). eRF1 and eRF3 form a complex in the terminating ribosome, as revealed in the cryoEM structure of the mammalian eukaryotic release factor eRF1–eRF3-associated termination complex (14,15), as well as in structural studies of the eRF1–eRF3 complex (16). Crystal and EM structures of mammalian ribosomal complexes containing eRF1 have also been recently described (17,18). In mammals, two distinct genes encode for eRF3a and eRF3b, which have differences in their N-terminal regions but both proteins can bind to eRF1 (19). eRF3 comprises a GTP-binding domain (G-domain) and two ß-barrel domains (domain 2/3) at the C-terminus (Figure 1A). Its GTPase activity is dependent on eRF1 and the ribosome.

During NMD, the SURF complex in the ribosome associates with the exon junction complex (EJC), a complex deposited 20–24 nt upstream of exon–exon junctions after splicing, through UPF2 and UPF3 (20–23). The interaction of UPF2 to the CH domain of UPF1 stimulates its helicase activity, which is essential to trigger the NMD response (20,21,23). The SMG1 kinase is responsible of UPF1 phosphorylation, an important event to recruit mRNA decay machineries, and which is stimulated by UPF2 and UPF3b (10,24,25). These macromolecular protein interactions are regulated by additional factors such as the RUVBL1/2 complex (26) and the DHX34 helicase (27).

UPF2 is a 148 kDa protein comprising three conserved MIF4G (middle domain of translation initiation factor 4G) domains (Figure 1A). The structure of MIF4G-1 and MIF4G-2 has been determined by X-ray crystallography, as well as the structure of the MIF4G-2 and MIF4G-3 domains in tandem, which showed a perpendicular orientation between both domains (28). Also, electron microscopy (EM) revealed the overall organization of full length UPF2 forming an open ring comprising the three MIF4G domains (29–31). MIF4G-3 interacts with UPF3b (58 kDa) as it is revealed in the crystal structure of MIF4G-3 bound to the RRM (RNA-recognition motif) domain of UPF3b (32) and in the EM structure of the UPF2–UPF3b complex (29,30). UPF2 also interacts directly with SMG1, but the function of this interaction remains unclear (28,31,33). Although UPF2 is proposed to associate with SURF as part of UPF3b–EJC complex, it can also form complex with UPF1 and SMG1 independently of UPF3b (10,31). Considering that some NMD events are independent of UPF3b and EJC (34–36), this opens the possibility that UPF2 could be directly recruited to SURF by multiple protein interactions including UPF1, SMG1 and others.

Here, we have characterized the interaction between human UPF2 and eRF3. Yeast Upf2p and eRF3p interact *in vitro* using purified proteins (37), but this interaction has not been studied, up to our best knowledge, in mammals. We demonstrate biochemically and structurally that eRF3 is a direct partner of UPF2 and that binding of UPF2 to UPF3b interferes with the formation of the UPF2–eRF3 complex. eRF1–eRF3 is part of the SURF complex, assembled during NMD initiation, suggesting that UPF2 could be recruited to SURF and the ribosomes, which we corroborate using pull down experiments and UPF2 mutants with reduced affinity for UPF3. These results, together with those of others, suggest that UPF2 has the potential to interact with several NMD factors, including eRF3 at the ribosome, UPF3b at the EJC, as well as UPF1 and SMG1. It is unlikely that UPF2 can engage in all those interactions simultaneously, and therefore, UPF2 possibly transfers through several transient complexes, where it may contribute to organize the order of events regulating NMD.

MATERIALS AND METHODS

Expression and purification of proteins in *E. coli*

UPF2 and UPF3b were produced as described in Melero *et al*. (29). The RRM domain of UPF3b (residues 42–143) and several fragments of UPF2 ($UPF2^{761\text{-}1054}$ and $UPF2^{761\text{-}1227}$), were expressed and purified as described previously (22). Constructs $UPF2^{121\text{-}486}$ and $UPF2^{455\text{-}757}$ were expressed in *Escherichia coli* BL21 (DE3) cells and purified through its N-terminal His-tag following a similar protocol, including the removal of the tag by TEV protease digestion.

eRF3a (CBP-eRF3a-His) and eRF1 (His-eRF1) were expressed in BL21(DE3)pLysS cells grown in LB supplemented with 25 mg/ml kanamycin at 37°C and expression induced with 1 mM IPTG (final concentration) at 20°C overnight. Cells were lyzed in 70 mM Tris (pH 8.0), 300 mM KCl, 5% (v/v) glycerol, 1 mM PMSF, 0.1% (v/v) Triton X-100 containing a cocktail of EDTA-free proteases inhibitors (Roche). Lysate was cleared by centrifugation at 35 000 rpm for 30 min at 4°C, and the supernatant was applied to a HisTrap HP column (GE Healthcare) equilibrated in buffer containing 70 mM Tris (pH 8.0), 300 mM KCl, 5% (v/v) glycerol and 40 mM imidazole. Elution was performed using a 40–500 mM imidazole gradient and fractions containing eRF1 or eRF3 were pooled and dialyzed overnight in buffer A without imidazole for eRF1, or in buffer A without imidazole but supplemented with 2 mM $CaCl_2$ for eRF3a. eRF3a was incubated with calmodulin affinity resin (Agilent Technologies) for 2 h at 4°C on a rotating platform, and eluted with 70 mM Tris pH 8.0, 300 mM KCl and 2 mM EGTA. Finally, proteins were applied to a Superdex 200 PC 3.2/30 column (GE Healthcare) equilibrated in 70 mM Tris (pH 8.0), 300 mM KCl, 5% (v/v) glycerol and 1 mM DTT. Purification of both proteins was monitored by sodium dodecyl sulphate-polyacrylamide gel electrophoresis (SDS-PAGE) and SimplyBlue (Novex) staining.

Expression of proteins in human cells

The pEF_Flag-HA-SBP-UPF1, pEF_Flag-HA-SBP-UPF2, pEFh_SBP-UPF2, pEFh_SBP-eGFP and pEFh_HA-SBP-MBP plasmids were previously defined (31,38). UPF2 mutants expressing plasmids, pEFh_SBP-UPF2_164–765 (missing residues 1–163 and 766–1272),

pEFh_SBP-UPF2_2–1107 (missing residues 1107–1272), pEFh_SBP-UPF2_d904–1015 (missing residues 904–1015), pEFh_SBP-UPF2_d1016–1107 (missing residues 1016–1107) and pEFh_SBP-UPF2_d802–903 (missing residues 802–903) were generated by standard cloning procedures. pSRD_UPF1 (non-tagged, residues 1–1129) was generated using restriction enzyme digestion protocol. pEFh_SBP-UPF3b and pEFh_HA-SBP-UPF3b were generated from codon optimized cDNA of human UPF3b (residues 2–483) (Life Technologies). Mouse eRF3b (residues 2–632) was polymerase chain reaction amplified from pFlag-CMV-2_GSPT2 (39) and cloned to generate pEFh_SBP-eRF3b and pEFs_HA-SBP-eRF3b.

Flag-HA-SBP-UPF1, Flag-HA-SBP-UPF2, Flag-HA-SBP-UPF2:UPF1 complex, Flag-HA-SBP-MBP, SBP-UPF2, SBP-UPF3b, SBP-eRF3b, SBP-eGFP and SBP-MBP were purified as described before (40). In brief, 293T cells were co-transfected with plasmids listed above using polyethyleneimine (Polysciences). After transfection, cells were lysed in NF-lysis buffer [20mM Tris (pH 7.5), 150 mM NaCl, 0.25 M Sucrose, 0.5% (v/v) NP-40, 1% (v/v) Tween 20] containing 1 mM DTT, protease inhibitor cocktail (Nacalai Tesque), phosphatase inhibitor cocktail (EDTA free) (Nacalai Tesque) and 50 μg/ml RNase A. SBP-tagged proteins were captured by Streptavidin Mag Sepharose (GE Healthcare) and eluted with T buffer (20 mM HEPES (pH 7.5), 150 mM NaCl, 2.5 mM $MgCl_2$, 0.05% (v/v) Tween 20) containing 1 mM DTT, protease inhibitor cocktail (EDTA free) (Nacalai Tesque), phosphatase inhibitor cocktail (Nacalai Tesque) and 2 mM biotin (Sigma-Aldrich). All SBP-UPF2 versions generated for this work was produced and purified using an identical protocol as that described above.

Interaction assays by size exclusion chromatography (SEC)

Purified proteins and complexes were pre-incubated at 30°C for 30 min with agitation and subsequently loaded on a Superdex 200 PC 3.2/30 column (GE Healthcare) equilibrated with 20 mM Tris (pH 7.4), 150 mM NaCl, 1 mM DTT, 1 mM $MgCl_2$ and 5% (v/v) glycerol. For the experiments described in Figure 1, UPF2 (5.7 μg) was either incubated with UPF3b (6 μg), eRF1 (5 μg) (1:2.65 UPF2/UPF3b molar ratio) or eRF3a (4 μg) (1:1.5 UPF2/eRF3a molar ratio), in 50 μl reaction and the mixtures were fractionated by size exclusion chromatography (SEC). Fractions containing the proteins were analyzed by SDS-PAGE and Oriole Fluorescent Gel Stain (Bio-Rad).

In vitro pull down experiments

For *in vitro* protein-binding assays, 3×10^7 of 293T cell extracts transfected with pEFs_HA-SBP-eRF3b, pEFs_HA-SBP-UPF3b or pEFs_HA-SBP-MBP plasmids were lysed in NF buffer containing 50 μg/ml RNase A and incubated with 0.5 mg of anti-HA-tag mAb-Magnetic beads (TANA2, MBL) for 2 h at 4°C. The beads were washed with T buffer and separated into 5–6 tubes. The separated beads were incubated with 200 nM of SBP-UPF2 wild-type (wt) or its derivatives (experiments in Figure 3), or 200 nM of SBP-UPF2 pre-incubated with 200 or 400 nM SBP-UPF3b (experiments in Figure 4) for 30 min in T buffer supplemented with 1 mM $MgCl_2$, 1 mM $MnCl_2$, 1 μM $ZnCl_2$, 1 mM DTT and 0.0025% (w/v) BSA. In Figure 2, 600 nM SBP-eGFP or SBP-eRF3b were mixed with 200 nM of the indicated Flag-HA-SBP-tagged proteins for 1 h. Then, mixtures were incubated with 0.5 mg of anti-HA-tag mAb-Magnetic beads. In Figure 6, 30 nM Flag-HA-SMG1C and 90 nM HA-UPF1/SBP-UPF2 complex were pre-assembled and immobilized with Flag-M2-Mag-beads (Sigma-Aldrich). Then, increasing amounts of UPF3b (9, 30 and 90 nM) were added. After 2 h of incubation, the beads were washed two times with T buffer containing 1 mM DTT. The bound proteins were eluted with SDS sample buffer lacking reducing agents. After addition of reducing agents and heat denaturation, the eluted proteins were separated by SDS-PAGE and stained using Oriole Fluorescent Gel Stain (Bio-Rad). Experiments were performed three times, and typical results are shown.

Immunoprecipitation of HA-tagged-UPF2 from HeLa TetOff cells and western blot analysis

The pSR_HA-UPF2, pSR_HA-UPF2-E858R and pSR_HA-UPF2-dU3 plasmids were previously defined (10). For immunoprecipitation, HeLa TetOff cells were transfected with the indicated plasmids using Lipofectamine LTX (Invitrogen). Two days after transfection, cells were lysed with a loose-fit Potter-Elvehjem Homogenizer in T-buffer with 50 μg/ml RNase A. Lysates were incubated with 1.5 μg of anti-HA rat monoclonal antibody (3F10, Roche) at 4°C for 1 h, mixed with 2 mg of protein-G-Dynabeads (Life technologies) and incubated at 4°C for 40 min. After washing with RNase(-) T-lysis buffer, the beads were eluted with SDS sample buffer containing 50 mM DTT. Eluted proteins were separated by SDS-PAGE and analyzed by western blot with the indicated antibodies. Experiments were performed three times, and typical results are shown.

Interaction assays using bio-layer interferometry (BLI)

The interaction between UPF2, either full-length or several fragments, with eRF3a, eRF3b and UPF3b was analyzed using a single channel BLItz system with Ni-NTA biosensors (ForteBio, Menlo Park, CA, USA). His-tagged ligand proteins, either UPF2, eRF3a or UPF3b, were immobilized through their His-tag on the sensors, at a final concentration of 6.75, 4 and 20 μM respectively in 70 mM Tris (pH 8.0), 300 mM KCl, 15% (v/v) glycerol and 1 mM DTT. Biolayer interferometry (BLI) experiments were performed at ambient temperature and shake speed of 2200 rpm, with baseline for 30 s followed by an association phase (experimental sample) for 300 s and a dissociation phase (buffer alone) for 300 s. The interacting proteins in analyte solutions were added at several concentrations to generate the sensorgrams and estimate the affinity constant (K_D), using the BLItz Pro software in a global manner using a simple 1:1 binding model. This software allowed a global analysis to determine a single pair of rate constants (K_a, K_d) for net binding and dissociation, the equilibrium dissociation constant ($K_D = K_d/K_a$), as well as the goodness of fit (R^2). A control experiment using just buffer as analyte served as a blank for correction of sensorgrams.

Antibodies

Antibodies against SMG1, UPF1, UPF2, UPF3b and eIF4A3 were described previously (9,10,41). Antibodies against Flag (M2, Sigma), SBP (SB19-C4, SantaCruz), MLN51 (Sigma), Y14 (Abcam), Magoh (Abcam), rpS6 (Cell signalling technology), rpL7a (Cell signalling technology) and MBP (NEB) were obtained commercially. HeLa cell nuclear extracts were purchased from CILBiotech (Belgium).

EM and 3D reconstruction

Electron microscopy of UPF2-eRF3 was performed using a JEOL-1230 Transmission Electron Microscope operated at 100 kV after the samples were stained using 1% uranyl formate. Images of single molecules were recorded automatically at a final magnification of 2.28 Å per pixel using the F416 CMOS camera from TVIPS under the control of the EM-TOOLs program. A total of 143366 images were automatically extracted from the micrographs and selected bad particles (noise and background) were identified and removed by 2D classification using RELION (42), ending with a dataset containing 73057 images (Supplementary Figure S1). After a new round of 2D classification, we detected a number of images corresponding to UPF2 by comparing with images of purified UPF2. The remaining data set was then refined, assuming that contained mostly images corresponding to UPF2–eRF3. Several methods were used to generate a collection of initial templates for refinement, a phantom blob with the approximate size of the UPF2–eRF3 complex, a low pass filter version of UPF2 (29), and a volume generated using reference-free averages of the complex and EMAN2 initial volume generator (command: e2initialmodel.py)(43) (Supplementary Figure S2). When starting refinement from a low pass filter version of UPF2 or a blob, first rounds of refinement used reference-free averages as input, since these have a better signal to noise ration, better suited to initiate refinement from references without much features. After several rounds, refinement was followed using single particles. Volumes converged to similar low-resolution solutions after some rounds of refinement, despite the bias introduced by the initial reference. Then, the preliminary model of UPF2–eRF3 obtained using EMAN2 initial volume generator (command: e2initialmodel.py)(43) was used as seed to search in 3D for images of free UPF2 using maximum-likelihood methods in RELION (42). After this 3D classification, 19053 images of UPF2 were found to still be part of the dataset (Supplementary Figure S1). These were removed and the remaining 54004 images of the UPF2–eRF3 complex were refined until convergence using EMAN (44) and the initial template obtain from the EMAN2 initial volume generator. After refinement, the images processed showed a good distribution of Euler angles (Supplementary Figure S3). The resolution of the structure was estimated as 20.0 Å, using the Fourier Shell Correlation method and a 0.5 correlation coefficient (Supplementary Figure S3). Atomic structures of MIF4G domain 1 (MIF4G-1) and the tandem MIF4G2–3 of UPF2 (28), and the model of eRF3a (residues 207–634) (14) were fitted within the EM structure of UPF2–eRF3 using UCSF Chimera (45) (cross-correlation = 0.9461, 0.8833 and 0.8124, respectively). We were unable to define the handedness of the final structure. One hand was used for representation, but the opposite hand cannot be discarded.

Whole cell extract preparation, *in vitro* splicing and immunoprecipitation

HEK293T cells were transfected with Flag-pcDNA3 vector, Flag-UPF1, Flag-UPF2 or Flag-UPF3b plasmid (10). After 48 h incubation, transfected cells were harvested and whole cell extracts were prepared as previously described (46,47). Briefly, the transfected cells were harvested by pipetting and collected by low-speed centrifugation at ∼500 × *g* for 5 min, at 4°C. The resulting pellet was washed with ice-cold phosphate bufferedsaline (PBS) and re-suspended in ice-cold buffer E (20 mM HEPES-KOH (pH 7.9), 100 mM KCl, 0.2 mM EDTA, 10% (v/v) glycerol, 1 mM DTT). Typically, 200 μl of buffer E was used per 10 cm plate. Disrupt cells by sonication with an Ultrasonic processor Model ULTRA S. Homogenizer VP-5s (TAITEC, Japan). Sonication is carried out at 30% continuous for 5 s three times and 30 s incubation on ice between bursts. The sonicated lysate was centrifuged at 15 000 × *g*, 20 min at 4°C. The supernatant was saved as the whole cell extract. The substrates for *in vitro* splicing reaction were prepared as described previously. The *in vitro* splicing reactions in combination with HEK293T cell extracts were carried out essentially as reported previously (46,47). Briefly, a typical 50 μl splicing reaction with 2 × 10^5 cpm of ^{32}P-labeled transcripts contains 10 μl of HeLa cell nuclear extract (CILBIOTECH, Belgium) and 20 μl of HEK293T cell whole cell extract as well as 5 μl of 10 × SP buffer. Following 1 h incubation at 30°C, reaction mixture was diluted five times with RNA IP buffer [20 mM HEPES-NaOH (pH 8.0), 150 mM NaCl, 0.05% (v/v) Triton X-100] and immunoprecipitation with anti-Flag (M2, Sigma) antibody was performed using 200 μl of the mixture and 20 μl of M2 resin as described previously (46,47).

Polysome analysis

For polysome profile analysis, 2 × 10^7 of HeLa cell were washed with ice-cold PBS containing 50 μg/ml cycloheximide and harvested. Harvested cells were resuspended in 2 ml of cold reticulocyte standard buffer (RSB) [10 mM Tris (pH 7.5), 10 mM NaCl, 1.5 mM $MgCl_2$, 50 μg/ml cycloheximide, 2 μg/ml aprotinin, 2 mM PMSF]. Cell suspensions were separated in two tubes, and an equal volume of RBS buffer containing 1% (v/v) Triton X-100, 1% (v/v) deoxycholate, 2% (v/v) Tween 20 with or without 50 mM EDTA was added. The suspensions were Dounce homogenized and centrifuged for 30 min at 13 000 × *g*. A total of 1 ml of supernatant was loaded onto a linear gradient of 8 to 45% (w/v) sucrose in sucrose gradient buffer [10 mM Tris (pH 7.5), 75 mM KCl, 3 mM $MgCl_2$] and centrifuge in a SW40 rotor for 3 h at 36 000 rpm and 4°C. The gradient was collected from the bottom of the tube at 0.6 ml/min/tube. The A_{254}/UV was monitored with A254 filter set. To concentrate each fraction, sodium-deoxycholate

and trichloroacetic acid were added to final concentrations of 4 and 24% (v/v), respectively, and centrifuge 10 min at 13 000 × *g*. Precipitates were rinsed with 80% (v/v) acetone at −20°C and suspended by 1× SDS sample buffer containing 5% (v/v) β-ME. Fractions were separated by SDS-PAGE, and analyzed by western blot with the indicated antibodies. Experiments were performed twice, and typical results are shown.

RESULTS

Direct interaction between human UPF2 and eRF3

UPF2, eRF1 and eRF3 (eRF3a, one of the variants of eRF3; eRF3 from now on, unless specified) were expressed in *E. coli* and purified to homogeneity (Figure 1B). eRF3 and eRF1 were produced as tagged proteins, CBP-eRF3-His and His-eRF1 (named eRF3 and eRF1 through this manuscript, for simplicity). We analyzed if UPF2 could form a direct complex with eRF3 or eRF1 after incubating and resolving the proteins by SEC using a Superdex 200 PC 3.2/30 column (GE-Healthcare). Control experiments defined the elution profile for each of the individual proteins (Figure 1C). Then, UPF2 was either incubated with eRF3 or eRF1, and the mixture was fractionated using SEC. When UPF2 and eRF1 were mixed (1:2.65 molar ratio), the elution profile revealed two peaks, with similar elution times to those obtained for UPF2 (elution at 1.3 ml), and eRF1 (elution at 1.7 ml) injected individually and co-migration was not found when the fractions were analyzed by SDS-PAGE. Thus, UPF2 and eRF1 were not interacting under our experimental conditions (Figure 1D). On the other hand, when UPF2 and eRF3 were mixed (1:1.5 molar ratio), one peak eluted earlier than UPF2 injected alone (elution at 1.3 ml compared to 1.37 ml for UPF2 alone), and a significant shift in the elution profile of eRF3 was observed by SDS-PAGE of the fractions (Figure 1E). These observations suggested that UPF2 was forming a complex with eRF3 under our experimental conditions, whereas UPF2 did not interact with eRF1.

To further support that UPF2 and eRF3 can form a complex, we performed several pull down experiments using proteins expressed in human cells (Figure 2A). For this, HA (hemagglutinin) and SBP (Streptavidin Binding Peptide) tagged versions of UPF2 (Flag-HA-SBP-UPF2) and UPF1 (Flag-HA-SBP-UPF1) were produced in HEK 293T cells and enriched after affinity purification. We also produced UPF2 partially bound to UPF1 by co-expressing Flag-HA-SBP-UPF2 and untagged UPF1, following a similar strategy we used before (31). This time, our preparation showed only partial occupancy of UPF2, but all UPF1 co-purifying with UPF2 must be forming a complex with UPF2, since UPF1 was not tagged (Figure 2A; note that UPF1 and HA-SBP-UPF1 run differently in SDS-PAGE). The interaction between these proteins and eRF3 was studied by pull down through the HA tag using immobilized magnet beads. eRF3a aggregated when expressed in these cells, and thus we worked with eRF3b, produced as SBP-eRF3b (the use of eRF3b will be specified from now on; otherwise eRF3 stands for eRF3a), which did not aggregate (Figure 2A). All Flag-HA-SBP-tagged proteins did not precipitate SBP-eGFP (Figure 2B, lane 1–4, and 9–12, SBP-eGFP highlighted within a square). In addition, SBP-eRF3b did not interact with Flag-HA-SBP-tagged MBP (Figure 2B, lanes 5 and 13), ruling out that the interactions detected could be an artifact. We found that SBP-eRF3b interacted with UPF1 (Figure 2B, lane 6 and 14, pull down Flag-HA-SBP-UPF1 labeled with #, and co-precipitated eRF3b indicated within a square), as previously described (24), but also with UPF2 (Figure 2B, lane 7 and 15, co-precipitated eRF3b labeled within a square). The UPF2–UPF1 complex also interacted with eRF3b, indicating that the interaction of UPF1 and UPF2 is compatible with the binding to eRF3b (Figure 2B, lane 8 and 16).

UPF2 interacts with eRF3 less strongly than with UPF3

We measured the affinity constant for the interaction between UPF2 and eRF3 using BLI. A layer of eRF3a was immobilized on a biosensor tip using the His tag, and several concentrations of UPF2 were used to calculate an affinity constant (K_D) of 2.18 ± 0.5 μM (Figure 2C, Table 1). Values were also calculated for the eRF3b isoform purified from human cells, but this time, a His-tagged version of UPF2 was immobilized on the biosensor tip and SBP-eRF3b was used (K_D = 6.27 ± 3.05 μM; Table 1). We also calculated the K_D for the interaction between UPF2 and UPF3b using a similar experimental set up (Table 1). The values for the UPF2-UPF3b affinity constant obtained here (K_D = 0.02 ± 0.01 μM) (Figure 2D, Table 1) were in the same range as those described before using Surface Plasmon Resonance (22). Interestingly, the interaction between UPF2 and UPF3b was significantly stronger than between UPF2 and eRF3.

eRF3 binds to the C-terminal region of UPF2

A series of SBP-tagged UPF2 constructs and mutants and HA-SBP-eRF3b were used to narrow down what region in UPF2 is involved in contacting eRF3b in pull down experiments (Figure 3A and Bi). UPF2 (164–765), a large fragment of UPF2 comprising MIF4G-1 and MIF4G-2 did not show a significant interaction with eRF3b when compared with wt UPF2, suggesting that the UPF2–eRF3b interaction surface is mostly placed at the C-terminus of UPF2 (Figure 3C, lane 2 and 9; note that UPF2 (164–765) runs faster in the SDS-PAGE). In agreement with this, the UPF2 (Δ1016–1107) truncation reduced binding to eRF3b significantly compared to wt UPF2 (Figure 3C, lanes 5 and 12), confirming that UPF2–eRF3 interaction surface is placed at the UPF2 C-terminal region. Together, these experiments indicated that the C-terminal end of UPF2, around the MIF4G-3 domain, defines an important region to maintain the interaction between UPF2 and eRF3b. This would be compatible with the interacting surface between UPF2 and eRF3b involving a larger region around domain MIF4G-3 and the C-terminus of UPF2.

These results were further confirmed using four fragments of UPF2, expressed and purified from *E. coli*, $UPF2^{121\text{-}486}$, $UPF2^{455\text{-}757}$, $UPF2^{761\text{-}1054}$ and $UPF2^{761\text{-}1227}$, and corresponding approximately to domain MIF4G-1, MIF4G-2, MIF4G-3 and MIF4G-3 plus regions at the C-terminus of this domain (Figure 3Bii). The interaction be-

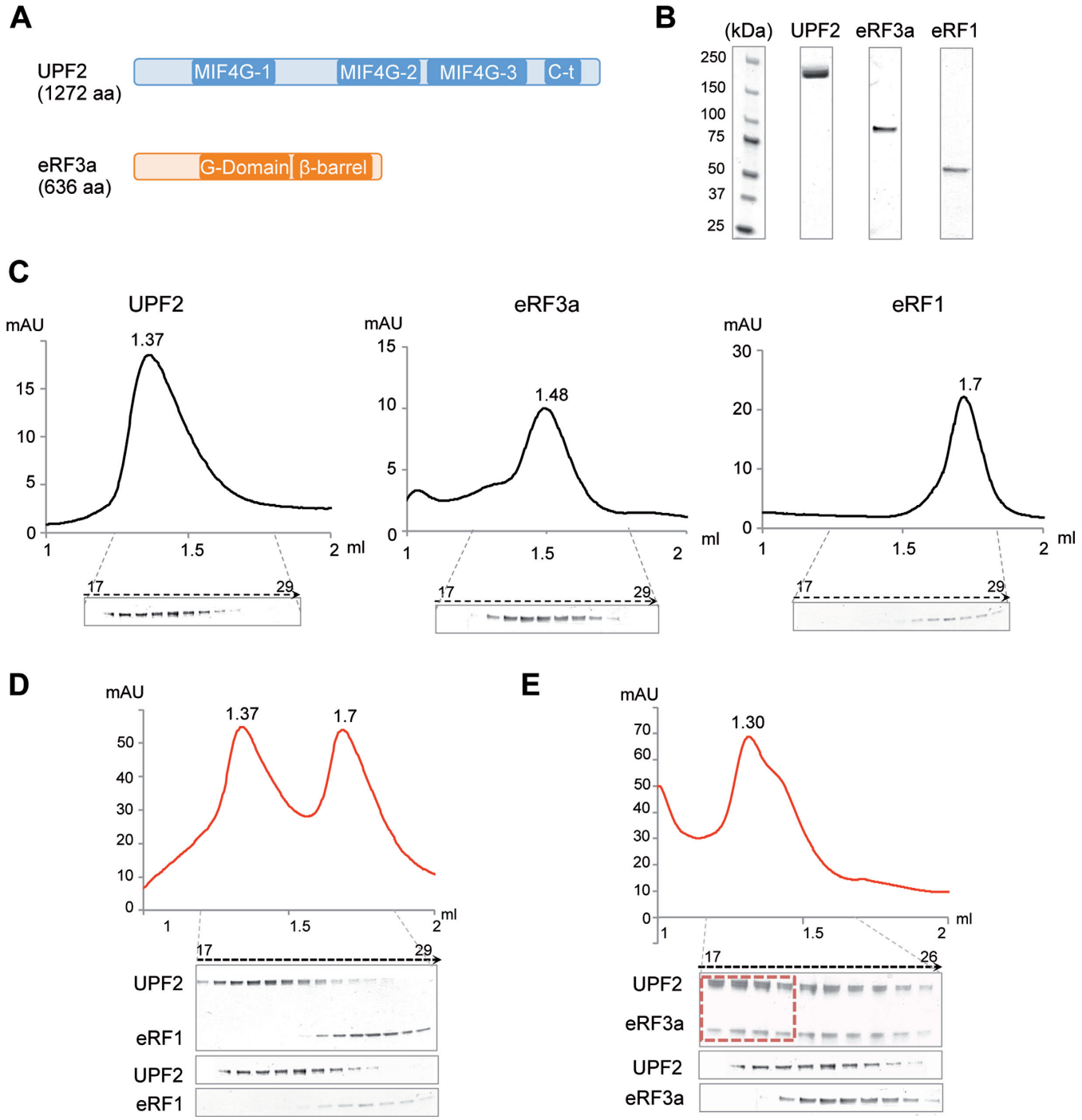

Figure 1. UPF2 interacts with eRF3 *in vitro*. (**A**) Schematic representation of the sequence and domain arrangement in human UPF2 and eRF3a. Regions obtained from known crystal structures or homology models (in case of MIF4G-1 and MIF4G-2 in UPF2) are indicated. The MIF4G domains of UPF2 are colored in blue, and the G-domain and the ß-barrel domain of eRF3a are in orange. (**B**) Sodium dodecyl sulphate-polyacrylamide gel electrophoresis (SDS-PAGE) and SimplyBlue (Novex) staining of purified UPF2, eRF3 and eRF1 used in these studies. Molecular Weight markers are indicated (kDa). (**C**) Size exclusion chromatography (SEC) of purified UPF2, eRF3a and eRF1. Elution volumes are indicated on top of the peaks (in ml). Bottom panels show SDS-PAGE and SimplyBlue (Novex) staining of the fractions containing the peaks in each case. (**D** and **E**) SEC experiments to analyze the potential interaction of UPF2 with eRF1 (D) and with eRF3a (E). A mixture of UPF2 and either protein was loaded onto the column and fractionated as in (C). Bottom panels show SDS-PAGE and SimplyBlue (Novex) staining of the fractions containing the peaks in each experiment, and below these, the fractions corresponding to the proteins analyzed individually under similar conditions, to help the comparison. UPF2 co-migrated with eRF3 in high molecular weight fractions (highlighted within a red square) compared to the control runs.

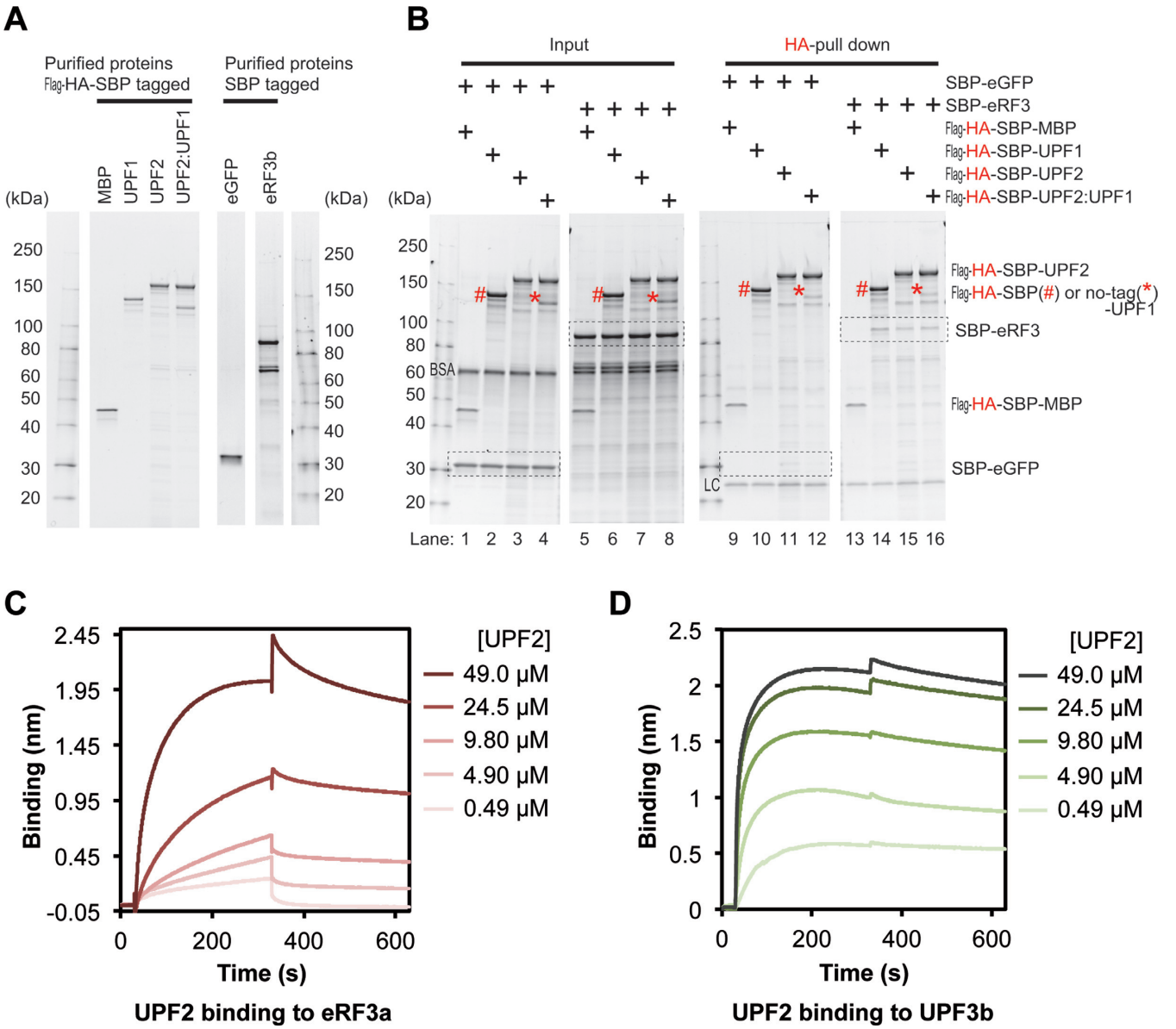

Figure 2. UPF2 interacts with eRF3. (**A**) SDS-PAGE and Oriole Fluorescent Gel Stain (Bio-Rad) staining of purified HA-SBP-tagged and SBP-tagged proteins used for the interaction assays. (**B**) HA-pull down experiments to test the interaction of Flag-HA-SBP-UPF1 and Flag-HA-SBP-UPF2 with SBP-eRF3b. Controls using Flag-HA-SBP-MBP and SBP-eGFP were used to discard artifacts. Input and pull down material were analyzed by SDS-PAGE and Oriole Fluorescent Gel Stain (Bio-Rad). For clarity, eRF3b and SBP-eGFP in the input and co-precipitated material are highlighted within a square. HA-SBP-UPF1 (#) and non-tagged UPF1 (*) are also indicated. Non-tagged UPF1 in the HA-SBP-UPF2:UPF1 complex decreased in both eGFP control pull down (lane 4) and eRF3b pull down (lane 8), suggesting that some UPF1 in the complex is washed out during experiment. BSA in the input material is indicated. LC indicates the positions of IgG light chain. (**C**) Sensorgrams from bio-layer interferometry (BLI) experiments performed to estimate the affinity constants for eRF3a-UPF2 complex. eRF3a was immobilized to the tip of the sensor through its His-tag (ligand) and increasing concentrations of UPF2 (analyte) were tested for interaction. (**D**) Sensorgrams as in (C), but for the interaction between UPF3b (ligand) and UPF2 (analyte).

tween UPF2 fragments and eRF3 was analyzed by BLI, revealing that only the C-terminal fragments of UPF2 interacted significantly with eRF3. Interestingly, the same UPF2 constructs that interacted with eRF3 were also found to be capable of binding to UPF3b (Figure 3D, Table 1).

Taken together, these results clearly show that UPF2 and eRF3 interact, and that the region of interaction involves the C-terminal end of UPF2, around the third MIF4G domain, which is at least partially coincident with the regions involved in UPF3b binding.

3D structure of the UPF2–RF3 complex

The UPF2–eRF3 complex was then reconstituted by mixing UPF2 and eRF3. The complex was resolved by SEC, and the peak fraction corresponding to elution volume 1.3 ml and containing both proteins (Figure 1E) was observed in the electron microscope after staining with 1% (w/v) uranyl formate to help visualizing the complex. The molecular weight and dimensions of the UPF2–eRF3 complex are relatively small to be easily visualized and resolved by cryo-EM of vitrified samples, where the signal of the complex

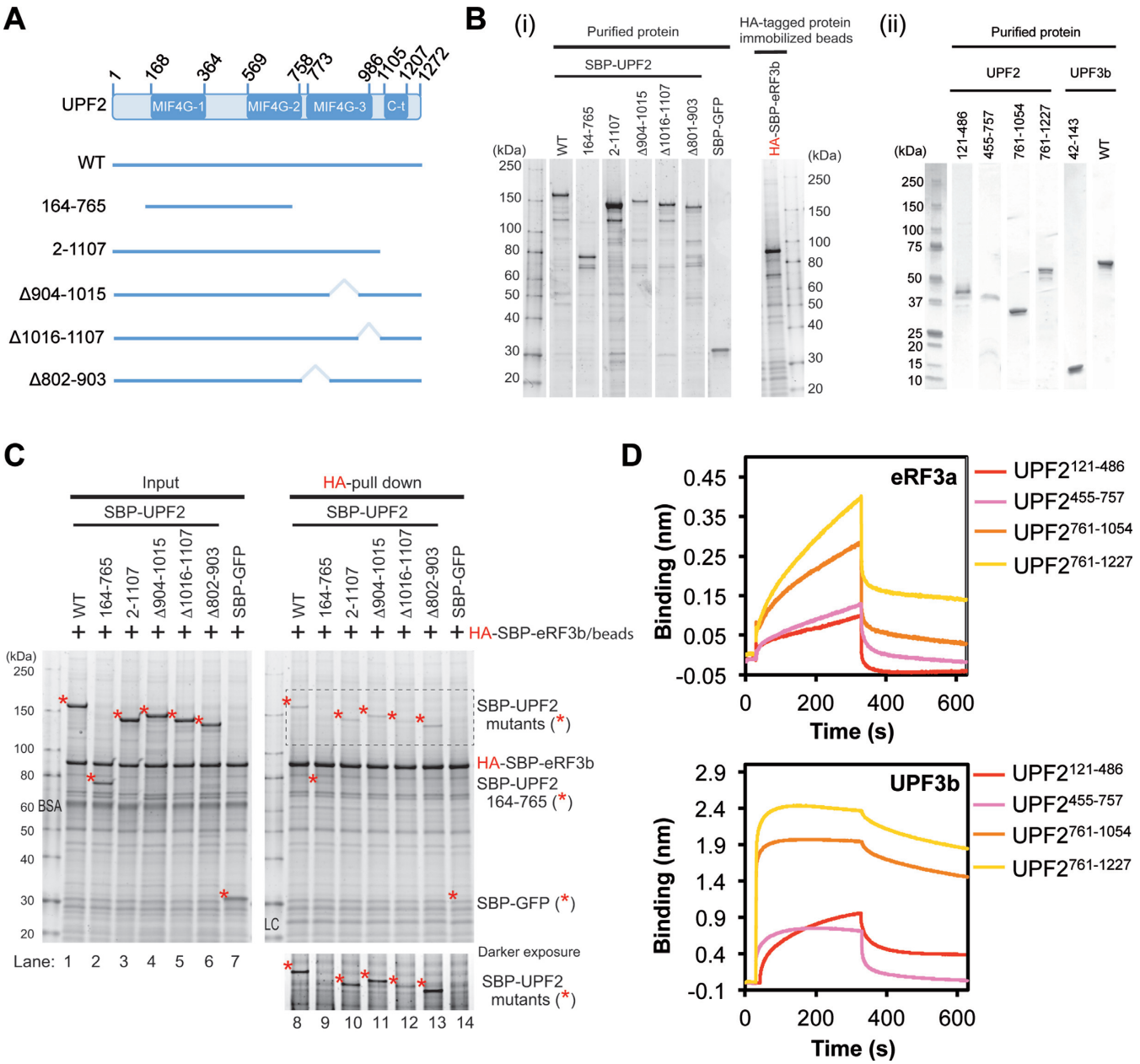

Figure 3. eRF3 binds the C-terminal region of UPF2. (**A**) Schematic representation of several SBP-tagged versions of UPF2 used for the interaction assays. (**B**) (i) SDS-PAGE and Oriole Fluorescent Gel Stain (Bio-Rad) staining of purified SBP-tagged versions of UPF2 used for the interaction assays (left panel), and 20% of HA-SBP-eRF3b bound to anti-HA magnetic beads and eluted with SDS sample buffer (right panel). Molecular Weight markers are indicated (kDa). (ii) SDS-PAGE and SimplyBlue (Novex) staining of purified fragments of UPF2 produced in *Escherichia coli* ($UPF2^{121-486}$, $UPF2^{455-757}$, $UPF2^{761-1054}$ and $UPF2^{761-1227}$, corresponding approximately to domain MIF4G-1, MIF4G-2, MIF4G-3 and MIF4G-3 plus regions at the C-terminus). Molecular Weight markers are indicated (kDa). (**C**) HA-pulldown experiments to test the interaction of the SBP-tagged versions of UPF2 shown in (A) and HA-SBP-eRF3b. HA-SBP-eRF3b immobilized on anti-HA magnetic beads were incubated with SBP-eGFP (as control, lanes 4 and 14), SBP-UPF2 wild-type (wt) (lanes 1 and 8) or its derivatives (400 nM each) (lanes 2–6 and 9–13). A total of 50% of input and 50% of precipitated materials were subjected to SDS-PAGE and stained with Oriole Fluorescent Gel Stain (Bio-Rad). Asterisk (*), BSA and LC indicate the positions of UPF2 wt and its derivatives, BSA and IgG light chain, respectively. Note that SBP-UPF2 (164–765) runs faster than the rest of UPF2 mutants. The region within a square is shown below in a darker exposure to highlight the presence of UPF2 mutants. SBP-UPF2 (164–765) does not appear here as it is run in a different position in the gel. Molecular Weight markers are indicated (kDa). (**D**) Sensorgrams from BLI experiments to test the interaction between eRF3a (upper panel) or UPF3b (bottom panel) to the indicated constructs of UPF2 ($UPF2^{121-486}$, $UPF2^{455-757}$, $UPF2^{761-1054}$ and $UPF2^{761-1227}$) at a final concentration of 8 μM. Experiments were performed three times for the calculation of kinetic parameters and a typical sensorgram for each condition is shown.

Table 1. Kinetic parameters measured by BLI for the interaction of eRF3a, eRF3b and UPF3b with UPF2 and several constructs of UPF2

Ligand	Analyte	K_D (M)	k_a ($M^{-1}\cdot s^{-1}$)	k_d (s^{-1})	R^2
eRF3a	**UPF2 WT**	$2.18 \pm 0.51\cdot10^{-6}$	$3.24\cdot10^{2}$	$6.89\cdot10^{-4}$	0.98
	UPF2$^{121\text{-}486}$	$2.69 \pm 3.77\cdot10^{-2}$	$2.31\cdot10^{1}$	$1.49\cdot10^{-2}$	0.95
	UPF2$^{455\text{-}757}$	$1.32 \pm 0.30\cdot10^{-4}$	$9.34\cdot10^{1}$	$1.17\cdot10^{-2}$	0.93
	UPF2$^{761\text{-}1054}$	$3.66 \pm 0.44\cdot10^{-5}$	$9.19\cdot10^{1}$	$3.34\cdot10^{-3}$	0.95
	UPF2$^{761\text{-}1227}$	$1.64 \pm 0.66\cdot10^{-5}$	$1.91\cdot10^{2}$	$2.95\cdot10^{-3}$	0.95
	UPF3b WT	$1.12 \pm 1.11\cdot10^{-5}$	$6.24\cdot10^{3}$	$4.54\cdot10^{-2}$	0.98
	UPF3b$^{42\text{–}143}$	$5.18 \pm 2.41\cdot10^{-5}$	$1.30\cdot10^{2}$	$5.99\cdot10^{-3}$	0.92
UPF3b	**UPF2 WT**	$2.07 \pm 1.59\cdot10^{-8}$	$4.18\cdot10^{4}$	$5.83\cdot10^{-4}$	0.98
	UPF2$^{121\text{-}486}$	$2.74 \pm 0.31\cdot10^{-5}$	$4.77\cdot10^{2}$	$1.32\cdot10^{-2}$	0.95
	UPF2$^{455\text{-}757}$	$2.49 \pm 1.18\cdot10^{-5}$	$1.85\cdot10^{3}$	$4.02\cdot10^{-2}$	0.98
	UPF2$^{761\text{-}1054}$	$3.69 \pm 0.98\cdot10^{-8}$	$6.87\cdot10^{4}$	$2.51\cdot10^{-3}$	0.96
	UPF2$^{761\text{-}1227}$	$3.99 \pm 0.43\cdot10^{-8}$	$4.99\cdot10^{4}$	$1.99\cdot10^{-3}$	0.95
UPF2	**eRF3b**	$6.27 \pm 3.05\cdot10^{-6}$	$1.34\cdot10^{4}$	$4.20\cdot10^{-2}$	0.95

Affinity constant (K_D), rate constants (k_a, k_d) and the goodness of fit (R^2) values are the average of at least three independent experiments, using several concentrations for each BLI interaction assay.

has to be sufficiently good to detect and align the images during image processing. Larger complexes, such as ribosomes, are better targets for these single-molecule methods. Although there are a number of successful cases for small proteins, these experiments are still very challenging. Thus, we used a staining agent to increase the signal of the images and facilitate determining the 3D structure although at low resolution (Figure 4A).

Images of single molecules were extracted and these were computationally processed and classified (see 'Materials and Methods' section for details and Supplementary Figure S1). After classification, we found that a subset of images were identical to those obtained for UPF2 alone (29,30), whereas other molecule images were larger, as expected for the UPF2–eRF3 complex (Figure 4B). Averages of UPF2 revealed a round shape compatible with the open ring structure described for this protein (29,30) (Figure 4C). Interestingly, the averages for UPF2–eRF3 also showed a round region, but some additional density was attached (Figure 4C). This was interpreted as resulting from the interaction between UPF2 and eRF3.

A 2D and 3D classification strategy was designed to isolate the images of UPF2–eRF3 and remove those of free UPF2 still present in the peak of the SEC (Supplementary Figure S1). A total of 54004 images of UPF2–eRF3 were identified following this procedure and these were refined using angular refinement methods. To discard any bias during image processing, we used several templates as models to start image refinement, including models obtained without any information from previous structures and we also used only the images of the UPF2–eRF3 complex obtained here (Supplementary Figure S2).

The structure of UPF2–eRF3 solved at 20 Å resolution revealed a flat open ring with an additional density protruding (Figure 4D, Supplementary Figure S3). The open ring region was reminiscent of the ring structure defined for UPF2 before (29,30). To locate the position of UPF2 and eRF3 within the complex, we aligned the structures of UPF2 (29) and UPF2–eRF3 and we calculated a difference map that helped us to segment the structure. This subtraction identified two distinct regions within UPF2–eRF3, one matching UPF2 (Figure 4D, blue color), whereas the remaining density could then be assigned to eRF3 (Figure 4D, orange color). To estimate the mass occupied by each protein within the complex, we calculated the molecular mass of each segmented map individually using the *volume* command implemented in EMAN (44). This algorithm estimates the volume enclosed by the EM map, at a given threshold of visualization, assuming a protein density average of 1.35 g/ml (0.81 Da/A^3). By doing this, we estimated a mass of 168 kDa for the UPF2 region, and 72 kDa for eRF3, which correlated well with their predicted molecular weights (148 and 79 kDa, respectively).

At this resolution, UPF2 appeared segmented in three main regions of density that could correspond to the three MIF4G domains. One end of the UPF2 ring was bound to eRF3, which should correspond to the C-terminal half of UPF2, as we had determined biochemically (Figure 3D). The crystal structure of the MIF4G domains 2 and 3 in tandem form a rigid assembly where the two domains are placed orthogonally respect to each other (28) and this structure could be fitted within the end of the UPF2 ring bound to eRF3 (cross-correlation = 0.88) (Figure 4E).

Crystal structures of fragments of *Schizosaccharomyces pombe* eRF3 (residues 196–662; PDB ID: 1R5B) (48), and human eRF3 (residues 439–637; PDB ID: 3E1Y) (16) have been solved. The structure of eRF3 has also been determined at lower resolutions, as part of an eRF1/eRF3/GTP complex using SAXS (16), and as part of a complex with the ribosome (14,15). The cryoEM of the ribosomal pretermination complex associated with eRF1/eRF3 at a resolution of 9.7 Å, enabled to propose an atomic model of the eRF1–eRF3 complex using the available crystal structures and constrains introduced by the cryoEM structure (PDB ID: 3J5Y) (14). Residues 207–634 of eRF3 were modeled and the comparison between this model and the density assigned to eRF3 in the UPF2–eRF3 complex showed that the EM map had overall dimensions consistent with size of eRF3 (Figure 4E). Some density was still available in the EM map to account for the N-terminal region of eRF3 missing in the atomic model. Nonetheless, it is important to stress that the intention of this comparison was only to determine if the range of dimensions in the EM map were consistent with eRF3, since the resolution was insufficient

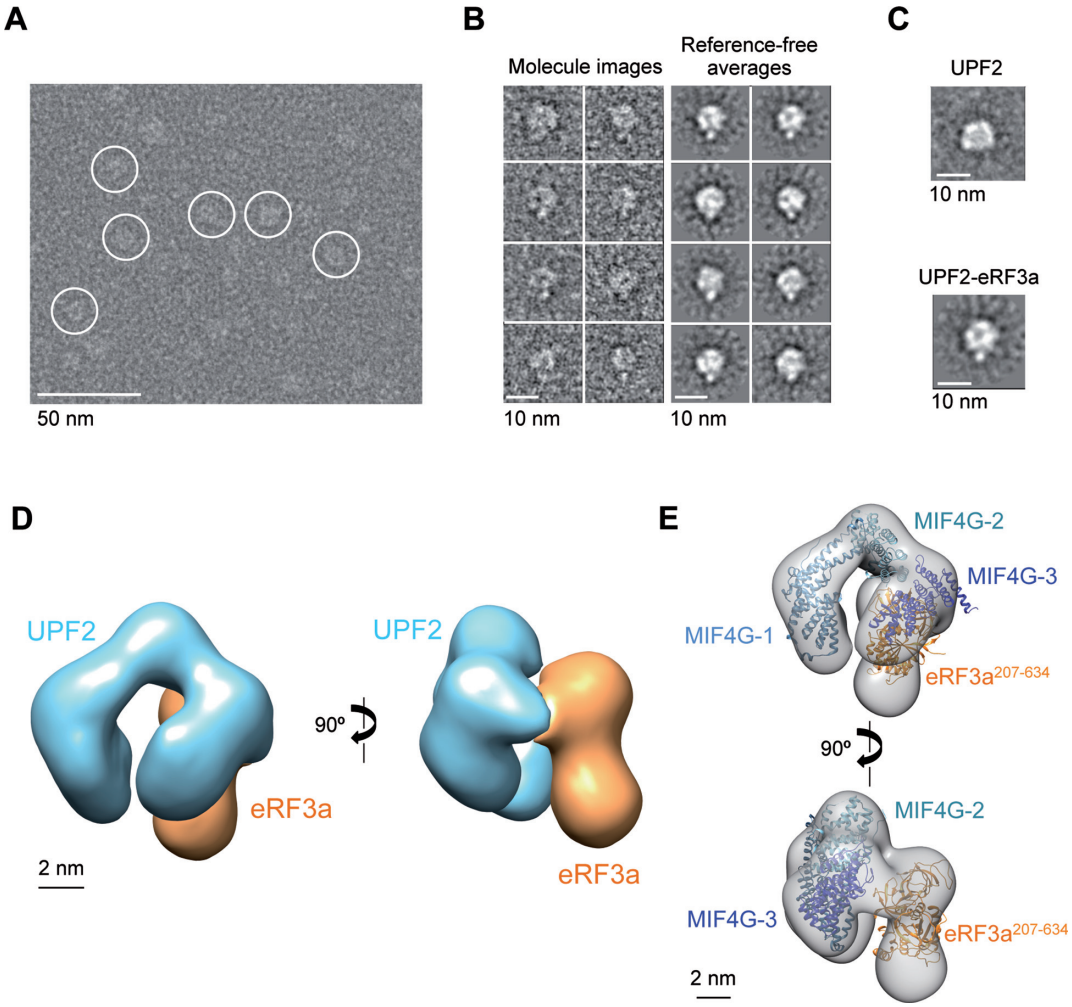

Figure 4. Electron microscopy of the UPF2–eRF3 complex. (**A**) Representative micrograph of the negative stained UPF2–eRF3a complex using the electron microscope. Scale bar represents 50 nm. (**B**) Images of single molecules obtained for the UPF2–eRF3a complex using EM. Right panels show some selected 2D reference-free averages obtained after alignment and averaging those images corresponding to views of the UPF2–eRF3a complex in similar orientation. Scale bar represents 10 nm. (**C**) Representative 2D averages for UPF2 and UPF2–eRF3a. Scale bar represents 10 nm. (**D**) 3D structure of UPF2–eRF3a where UPF2 and eRF3a components have been segmented and color differently (UPF2, blue color; eRF3a, orange color). Segmentation of the UPF2–eRF3a complex was performed using UCSF Chimera (45). Two views of the complex are shown. Scale bar represents 2 nm. (**E**) Fitting of atomic structures into the UPF2–eRF3a EM map. The 3D structure of UPF2–eRF3a is shown as a white transparent density with the crystal structures of UPF2 domains (28) and a model of eRF3 fitted. The eRF3 model corresponds to a fragment of eRF3 (residues 207–634) (PDB 3J5Y) (14,15). Scale bar represents 2 nm.

to define a precise orientation of eRF3 within the UPF2–eRF3 complex.

The interaction of UPF2 with UPF3b affects binding to eRF3

The structure of UPF2–eRF3 revealed some interesting features of this complex. First, eRF3 interacted preferentially with one of the two sides of the UPF2 open ring. Second, eRF3 occupied an area in UPF2 that could potentially partially overlap with the regions in UPF2 that bind to UPF3b (29). This was also suggested when analyzing the interaction of C-terminal fragments of UPF2 with eRF3 and UPF3b (Figure 3). Nonetheless, at 20 Å resolution (this study and Melero *et al.* (29)), it was not possibly to completely define if the side of the UPF2 ring involved in eRF3 binding is the same as the one proposed before to bind UPF3b (29).

Thus, we decide to analyze if UPF3b could interfere with binding of eRF3 to UPF2, using SBP-UPF2 and SBP-UPF3b purified from cells (Figure 5A), and HA-SBP-eRF3b, HA-SBP-UPF3b and HA-SBP-MBP that could be precipitated using the HA-magnetic beads (Figure 5B). As controls, we confirmed that HA-SBP-UPF3b (Figure 5C, labeled #) and HA-SBP-eRF3b could bind to SBP-UPF2, whereas HA-SBP-MBP did not precipitate SBP-UPF2, suggesting this experimental set up was not producing artifacts (Figure 5C). Note that the amount of UPF2 co-precipitated with eRF3b is much smaller than that of UPF3, in agreement with the K_D values obtained in BLI experiments. Interestingly, whereas HA-SBP-eRF3b could precipitate SBP-UPF2 (Figure 5C, lane 4 and 8, within a square), pre-incubation of SBP-UPF2 with SBP-UPF3b significantly reduced the interaction of SBP-UPF2 with HA-SBP-eRF3b

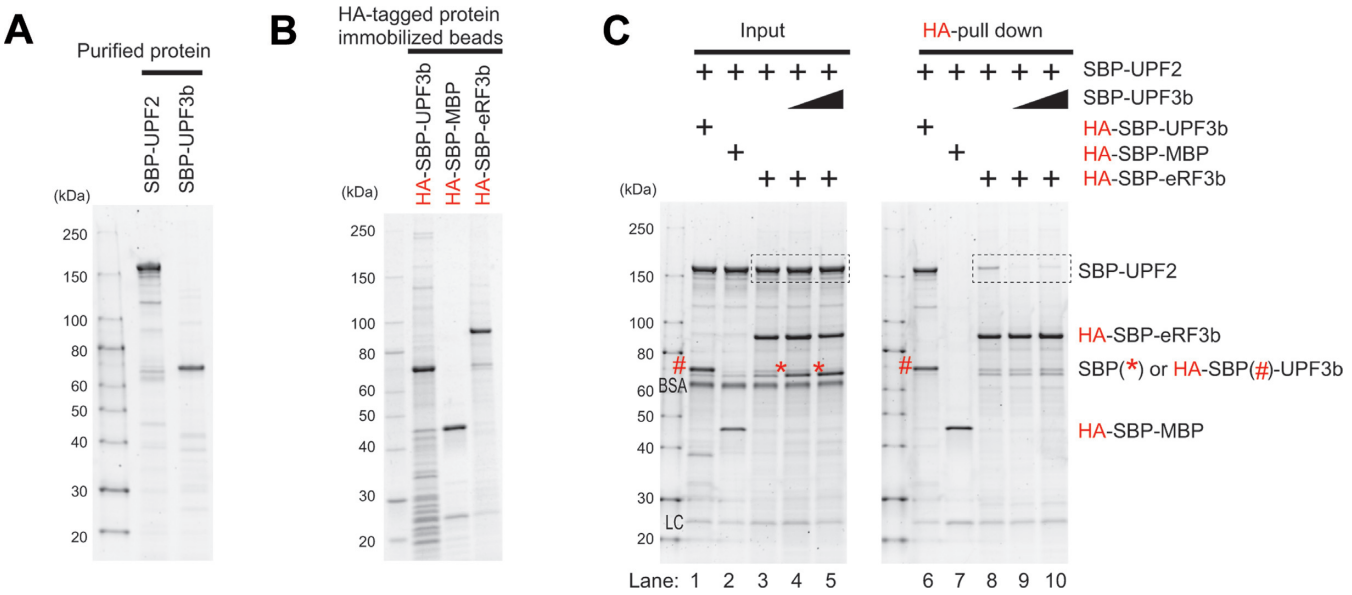

Figure 5. UPF3b binding to UPF2 affects recruitment of eRF3 to UPF2. (**A**) SDS-PAGE and Oriole Fluorescent Gel Stain (Bio-Rad) staining of purified SBP-UPF2 and SBP-UPF3b to be used in competition experiments in (**C**). (**B**) Purified HA-SBP-UPF3, HA-SBP-MBP and HA-BP-eRF3b were immobilized using magnetic beads. SDS-PAGE stained with Oriole Fluorescent Gel Stain (Bio-Rad) is shown. (C) Competition between UPF3b and eRF3b to bind UPF2 tested by HA-tag pulldown. HA-SBP-UPF3b (labeled #) and HA-SBP-eRF3b can pull down UPF2. Increasing amounts of SBP-UPF3b (labeled *) pre-incubated with SBP-UPF2, reduce the amount of SBP-UPF2 binding to HA-SBP-eRF3b. BSA in the input material is indicated. IgG light chain (LC) and molecular weight markers (kDa) are indicated. Experiments were analyzed by SDS-PAGE and Oriole Fluorescent Gel Stain (Bio-Rad) staining.

(Figure 5C, SBP-UPF3b labeled *, precipitated SBP-UPF2 indicated within a square). This indicated a stronger interaction between UPF2 and UPF3b than between UPF2 and eRF3. Taken together these results suggest that binding of UPF2 to UPF3b interferes with the binding of UPF2 to eRF3.

UPF2 associates with SURF in an UPF3-independent manner

According to a prevailing model for NMD initiation, UPF2 is recruited on post-spliced mRNAs as part of an UPF2–UPF3–EJC complex and the transient interaction of this UPF2–UPF3–EJC complex with SURF at the ribosome would stimulate SMG1-mediated UPF1 phosphorylation (1,2). However, our finding that UPF2 forms a direct complex with eRF3 provides an alternative pathway to recruit UPF2 on the ribosome. This would agree with recent evidence showing that UPF2 binds SURF components SMG1 and UPF1 in an UPF3-independent manner (10,28,31,33). To test this possibility, we analyzed if UPF2 could be directly recruited to SURF and the ribosome in cells. HA-tagged UPF2 (HA-UPF2) was expressed in HeLa TetOff cells and the associated proteins analyzed after immunoprecipitation using an RNAase A treatment to discard RNA-mediated interactions. We followed the input and precipitated material by Western blot (WB) using antibodies for markers of the SURF complex (SMG1 and UPF1), components of the UPF3–EJC complex (UPF3, MLN51, eIF4A3, Y14 and Magoh) and markers for the ribosome (ribosomal proteins rpS6 and spL7a). We found that in these cells wt UPF2 associated with the SURF complex, UPF3b and EJC components, as well as with ribosomal proteins (Figure 6A). The association of UPF2 with all these proteins could represent the assembly of DECID and the interaction of UPF3-EJC and SURF through UPF2 (2,9,10). Thus, it was important to test if UPF2 could be also recruited to SURF and ribosomes if it is not part of a complex with UPF3b and the EJC. When using UPF2-dU3 (in which residues 711–928 have been deleted) and UPF2-E858R, two UPF2 mutants with a reduced ability to bind UPF3b (10,49), the expected reduction in precipitation of UPF3b and the EJC was detected. Nevertheless, these mutants maintained a similar binding to SURF and ribosomal components than the wt protein (Figure 6A). In addition, we found that after polysome fractionation, UPF2 co-migrated with 80S ribosome in absence of EDTA, which disrupt 80S ribosome, (Figure 6B, left panel), or both 40S and 60S ribosomes in the presence of EDTA that disrupts 80S ribosome (Figure 6B, right panel), respectively. Together, these results indicated that UPF2 could associate to SURF and ribosome components in cells, in an UPF3–EJC-independent manner.

We further examined if UPF2 is part of the UPF3–EJC complex in post-spliced mRNAs by determining the association between Flag-UPF2 and EJC/mRNA in an *in vitro* splicing reaction coupled to immunoprecipitation analyses using HEK293T cell extracts (Figure 6C and D). UPF3, but not UPF1 and UPF2, preferentially associated with spliced mRNA after *in vitro* splicing, suggesting UPF2 might not necessarily be a constituent component of a putative UPF2–UPF3–EJC complex after splicing.

DISCUSSION

The activation of mRNA degradation by the NMD pathway is regulated by macromolecular interactions between

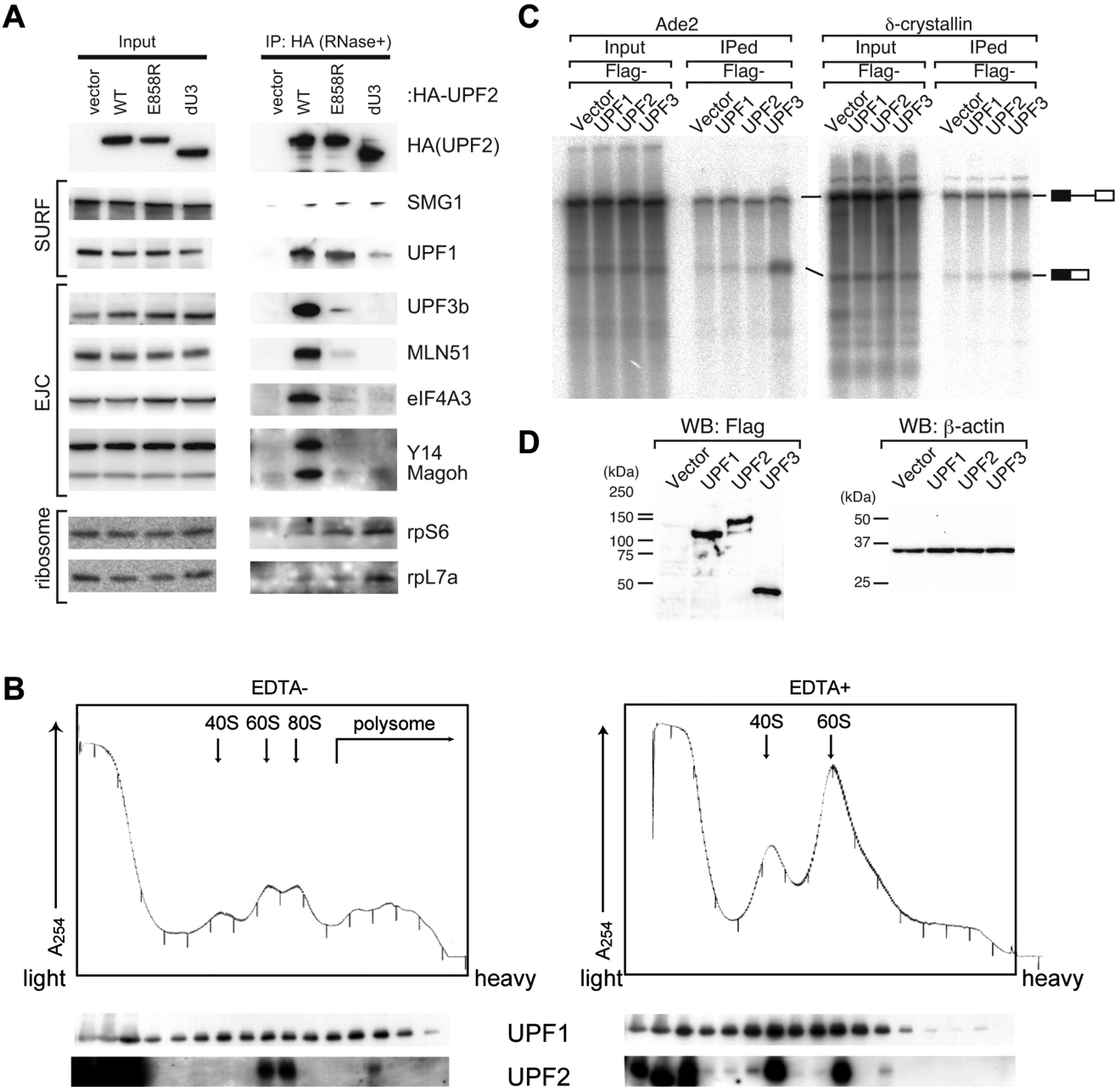

Figure 6. UPF2 is recruited to SURF in an UPF3-independent manner. (**A**) Proteins associating to UPF2 *in vivo*. HA-tagged UPF2 as well as the UPF2-dU3 and UPF2-E858R mutants affected in UPF3b binding were immunoprecipitated, and the associated proteins analyzed by western blot with the indicated antibodies. UPF2 associates to SMG1, UPF1, UPF3, ribosomal proteins (rpS6, rpL7a) and EJC components (MLN51, eIF4A3, Y14, Magoh). (**B**) Co-fractionation of UPF2 with ribosome. Cells were lysed in absence (left panel) or presence (right panel) of EDTA. 40S, 60S, 80S and polysomes were separated according to size in a 8–45% sucrose gradient. UV profile for detection of 40S, 60S, 80S and polysome are shown on top. Fractions were analyzed by western blot with the indicated antibodies (bottom panel). (**C**) Immunoprecipitation assay was carried out from an *in vitro* splicing reaction with ^{32}P-labeled Ade2 pre-mRNA (left panel) or with δ-crystallin pre-mRNA (right panel). For *in vitro* splicing, HeLa cell nuclear extracts were added to the whole cell extracts from HEK293T cells that had been transfected with control plasmid (Flag-vector), Flag-UPF1, UPF2 or UPF3b. RNAs precipitated by anti-Flag antibody (IP lanes) were analyzed by SDS-PAGE. Schematic representations of pre-mRNAs and mRNAs are shown on the right of the panel. Input lanes contain 5% of the total input material. (**D**) Analysis of the extracts from the cells transfected with control plasmid (Flag-vector), Flag-UPF1, UPF2 or UPF3b was performed by western blot with the indicated antibodies. Molecular Weight markers are indicated (kDa).

several protein factors, which are still not fully understood (2). In mammals, UPF2 is able to form a direct complex with several NMD factors, including UPF1, UPF3b and SMG1. Here we incorporate eRF3 as an additional UPF2-interacting factor by showing that human UPF2 and eRF3 can assemble a stable complex. Our study of the UPF2–eRF3 complex using EM, together with the biochemical analysis of the interaction of several fragments and mutants of UPF2 with eRF3, reveals that UPF2 forms an open ring, being mostly one side of UPF2 involved in the recognition of eRF3. MIF4G-3 in UPF2 interacts with the N-terminal RRM domain in UPF3b (32) and our structure suggests that at least some parts of this region could be also involved in eRF3 binding. Accordingly, truncation of residues 1016–1107 in UPF2 significantly reduce the interaction with eRF3, and the recombinant fragments of UPF2 comprising MIF4G-3 domain, $UPF2^{761\text{-}1054}$ and $UPF2^{761\text{-}1227}$, interact with eRF3 in interactions assays. This agrees with a potential binding site for eRF3p in Upf2p described in *Saccharomyces cerevisiae* (37). MIF4G domains participate as modules for the interaction with proteins in other contexts, such as the Not1-Not2-Not5 module of the yeast Ccr4–Not complex (50), and therefore it is conceivable that MIF4G domains in UPF2 can bind several partners. Our finding of a complex between UPF2 and eRF3 adds interesting insights to our understanding of the complexity of NMD regulation, mainly on (a) how UPF2 is recruited to the target mRNA and its mechanistic implications, and (b) the role of UPF2 as a platform for different complexes.

How the NMD factors are recruited to mRNAs containing PTCs is not completely understood. UPF1 would be recruited to stalled ribosomes through its interaction with the eukaryotic release factors eRF1 and eRF3 as part of the SURF complex (3,10). In addition, UPF1 can bind mRNAs but translation affects its distribution on the mRNAs (11–13). In mammals, UPF2 is presumed to bind the UPF3-EJC complex, but we show now that UPF2 binds also to eRF3 *in vitro*, and it associates with SURF and ribosomes in an UPF3 and EJC-independent manner in cells. In addition, unlike UPF3, UPF2 does not show preferential association for spliced mRNA after *in vitro* splicing. Therefore, UPF2 can be recruited to SURF through direct interaction with SMG1 (28,31), UPF1 (10) and eRF3, three of the four components of SURF.

A direct recruitment of UPF2 to SURF can have implications in our understanding of how NMD initiation takes place. An emerging view is that multiple pathways can converge in the activation of an NMD response with distinct requirements depending on organism, cell and transcript (51–53). Some NMD events in mammals are independent of a downstream EJC (34,35) and UPF3b (36). We show evidence that UPF2 can form a complex with SURF and ribosomal proteins independently of an EJC and UPF3. This could be interpreted as a model where UPF2 can be recruited to SURF first, rather than to UPF3–EJC, in addition to the previously proposed model implying formation of the UPF2–UPF3–EJC complex (1–3,23). This model might adapt to the faux 3′-UTR induced NMD, which is EJC independent and conserved among eukaryote including yeast, nematode and fly (2,35,53). Consistently, yeast Upf2p can be recruited to 80S ribosome in an *UPF3* independent manner (54).

Our results also highlight the role of UPF2 as a platform for protein interactions. UPF2 can bind many of the factors involved in the initial stages of the NMD response, such as UPF1, UPF3, SMG1 and eRF3p, but we show that not all of these can probably bind to UPF2 simultaneously. The regions of UPF2 involved in binding to eRF3 and UPF3b partially overlapped in the EM structure and binding of UPF2 to UPF3b affects binding to eRF3. Consistent with our results, yeast Upf3p and Upf2p competitively binds eRF3 *in vitro* (37). This is particularly interesting since eRF3 is bound to the stalled ribosome, whereas UPF3b is thought to bind to the EJC. UPF3b could eventually displace eRF3 from an UPF2–eRF3 complex, because UPF2 binds UPF3b with higher affinity than eRF3. The interaction of UPF2 with eRF3 or UPF3, when previously bound to the other partner, would probably require the displacement of the other protein. At this stage, the differences in affinities could be important. Similar findings have been found for instance in splicing factor CWC22 (Complexed With Cef1). CWC22 forms a complex with eIF4A3, which is incompatible with the binding of eIF4A3 to MAGO and Y14, two components of the EJC. Still CWC22 is required to escort eIF4A3 to spliceosomes and promote binding to MAGO and Y14 to assemble the EJC (55). It is worth mentioning that we have also found that eRF3 interacts with UPF3b and the RRM motif of UPF3b (Table 1). The binding of yeast eRF3p and Upf3p was also detected *in vitro* (37). Therefore, even if there is a clash between UPF3b and eRF3 when binding to UPF2, we cannot rule out that a tripartite complex containing UPF2, eRF3 and UPF3b could be formed if eRF3 and UPF3b can still interact when one of them is bound to UPF2. Consistent with this view, the DECID complex assembled during NMD has been shown to contain ribosome, the SURF complex, UPF2, UPF3 and EJC (9,41).

Initiation of the NMD response requires the concerted action of several factors. Here we describe an, up to our knowledge, previously uncharacterized interaction between human UPF2, one of these NMD factors and eRF3, together with evidence showing that UPF2 can be recruited directly to the SURF complex and a stalled ribosome. These interactions indicate that UPF2 possibly transits through several complexes and organizes events regulating the initiation of the NMD response. The direct recruitment of UPF2 to SURF and ribosomes could contribute to some EJC and/or UPF3-independent NMD events described in mammals.

SUPPLEMENTARY DATA

Supplementary Data are available at NAR Online.

ACKNOWLEDGEMENTS

We thank Shigeo Ohno (Yokohama City University, Japan) for providing reagents, constructs and protocols for the purification of SMG1C. We thank Elena Conti (MPI, Germany) for her help with UPFs, eRF1 and eRF3a. We thank Shin-ichi Hoshino for providing mouse eRF3b cDNA. We

thank Christiane Schaffitzel for providing the PDB file for the tandem MIF4G-2/MIF4G-3 domains. We also thank Isao Kashima (Tokyo University) for help with UPF2 western blotting in Figure 6B and Juan Roman Luque (CIB) for his help in the BLI experiments.

FUNDING

Spanish Ministry of Science and Innovation [SAF2011-22988, SAF2014-52301-R to O.L.; Juan de la Cierva contract JCI-2011-09536 to R.M.]; 'Red Temática de Investigación Cooperativa en Cáncer (RTICC)' from the 'Instituto de Salud CarlosIII' [RD06/0020/1001 to O.L., R.C.]; Japan Society for the Promotion of Science KAKENHI [20405020 TO A.Y.]; Takeda Science Foundation. Funding for open access charge: Spanish Ministry of Science and Innovation [SAF2014-52301-R].

Conflict of interest statement. None declared.

REFERENCES

1. Kervestin,S. and Jacobson,A. (2012) NMD: a multifaceted response to premature translational termination. *Nat. Rev. Mol. Cell Biol.*, **13**, 700–712.
2. Schweingruber,C., Rufener,S.C., Zund,D., Yamashita,A. and Muhlemann,O. (2013) Nonsense-mediated mRNA decay—mechanisms of substrate mRNA recognition and degradation in mammalian cells. *Biochim. Biophys. Acta*, **1829**, 612–623.
3. Yamashita,A. (2013) Role of SMG-1-mediated Upf1 phosphorylation in mammalian nonsense-mediated mRNA decay. *Genes Cells*, **18**, 161–175.
4. Behm-Ansmant,I., Kashima,I., Rehwinkel,J., Sauliere,J., Wittkopp,N. and Izaurralde,E. (2007) mRNA quality control: an ancient machinery recognizes and degrades mRNAs with nonsense codons. *FEBS Lett.*, **581**, 2845–2853.
5. Lykke-Andersen,S. and Jensen,T.H. (2015) Nonsense-mediated mRNA decay: an intricate machinery that shapes transcriptomes. *Nat. Rev. Mol. Cell Biol.*, **16**, 665–677.
6. He,F. and Jacobson,A. (2015) Nonsense-mediated mRNA decay: degradation of defective transcripts is only part of the story. *Annu. Rev. Genet.*, **49**, 339–366.
7. Lou,C.H., Shum,E.Y. and Wilkinson,M.F. (2015) RNA degradation drives stem cell differentiation. *EMBO J.*, **34**, 1606–1608.
8. Li,T., Shi,Y., Wang,P., Guachalla,L.M., Sun,B., Joerss,T., Chen,Y.S., Groth,M., Krueger,A., Platzer,M. *et al.* (2015) Smg6/Est1 licenses embryonic stem cell differentiation via nonsense-mediated mRNA decay. *EMBO J.*, **34**, 1630–1647.
9. Yamashita,A., Izumi,N., Kashima,I., Ohnishi,T., Saari,B., Katsuhata,Y., Muramatsu,R., Morita,T., Iwamatsu,A., Hachiya,T. *et al.* (2009) SMG-8 and SMG-9, two novel subunits of the SMG-1 complex, regulate remodeling of the mRNA surveillance complex during nonsense-mediated mRNA decay. *Genes Dev.*, **23**, 1091–1105.
10. Kashima,I., Yamashita,A., Izumi,N., Kataoka,N., Morishita,R., Hoshino,S., Ohno,M., Dreyfuss,G. and Ohno,S. (2006) Binding of a novel SMG-1-Upf1-eRF1-eRF3 complex (SURF) to the exon junction complex triggers Upf1 phosphorylation and nonsense-mediated mRNA decay. *Genes Dev.*, **20**, 355–367.
11. Hurt,J.A., Robertson,A.D. and Burge,C.B. (2013) Global analyses of UPF1 binding and function reveal expanded scope of nonsense-mediated mRNA decay. *Genome Res.*, **23**, 1636–1650.
12. Kurosaki,T. and Maquat,L.E. (2013) Rules that govern UPF1 binding to mRNA 3′ UTRs. *Proc. Natl. Acad. Sci. U.S.A.*, **110**, 3357–3362.
13. Zund,D., Gruber,A.R., Zavolan,M. and Muhlemann,O. (2013) Translation-dependent displacement of UPF1 from coding sequences causes its enrichment in 3′ UTRs. *Nat. Struct. Mol. Biol.*, **20**, 936–943.
14. des Georges,A., Hashem,Y., Unbehaun,A., Grassucci,R.A., Taylor,D., Hellen,C.U., Pestova,T.V. and Frank,J. (2014) Structure of the mammalian ribosomal pre-termination complex associated with eRF1.eRF3.GDPNP. *Nucleic Acids Res.*, **42**, 3409–3418.
15. Taylor,D., Unbehaun,A., Li,W., Das,S., Lei,J., Liao,H.Y., Grassucci,R.A., Pestova,T.V. and Frank,J. (2012) Cryo-EM structure of the mammalian eukaryotic release factor eRF1-eRF3-associated termination complex. *Proc. Natl. Acad. Sci. U.S.A.*, **109**, 18413–18418.
16. Cheng,Z., Saito,K., Pisarev,A.V., Wada,M., Pisareva,V.P., Pestova,T.V., Gajda,M., Round,A., Kong,C., Lim,M. *et al.* (2009) Structural insights into eRF3 and stop codon recognition by eRF1. *Genes Dev.*, **23**, 1106–1118.
17. Brown,A., Shao,S., Murray,J., Hegde,R.S. and Ramakrishnan,V. (2015) Structural basis for stop codon recognition in eukaryotes. *Nature*, **524**, 493–496.
18. Matheisl,S., Berninghausen,O., Becker,T. and Beckmann,R. (2015) Structure of a human translation termination complex. *Nucleic Acids Res.*, **43**, 8615–8626.
19. Chauvin,C., Salhi,S., Le Goff,C., Viranaicken,W., Diop,D. and Jean-Jean,O. (2005) Involvement of human release factors eRF3a and eRF3b in translation termination and regulation of the termination complex formation. *Mol. Cell. Biol.*, **25**, 5801–5811.
20. Chakrabarti,S., Jayachandran,U., Bonneau,F., Fiorini,F., Basquin,C., Domcke,S., Le Hir,H. and Conti,E. (2011) Molecular mechanisms for the RNA-dependent ATPase activity of Upf1 and its regulation by Upf2. *Mol. Cell*, **41**, 693–703.
21. Clerici,M., Mourao,A., Gutsche,I., Gehring,N.H., Hentze,M.W., Kulozik,A., Kadlec,J., Sattler,M. and Cusack,S. (2009) Unusual bipartite mode of interaction between the nonsense-mediated decay factors, UPF1 and UPF2. *EMBO J.*, **28**, 2293–2306.
22. Buchwald,G., Ebert,J., Basquin,C., Sauliere,J., Jayachandran,U., Bono,F., Le Hir,H. and Conti,E. (2010) Insights into the recruitment of the NMD machinery from the crystal structure of a core EJC-UPF3b complex. *Proc. Natl. Acad. Sci. U.S.A.*, **107**, 10050–10055.
23. Chamieh,H., Ballut,L., Bonneau,F. and Le Hir,H. (2008) NMD factors UPF2 and UPF3 bridge UPF1 to the exon junction complex and stimulate its RNA helicase activity. *Nat. Struct. Mol. Biol.*, **15**, 85–93.
24. Ivanov,P.V., Gehring,N.H., Kunz,J.B., Hentze,M.W. and Kulozik,A.E. (2008) Interactions between UPF1, eRFs, PABP and the exon junction complex suggest an integrated model for mammalian NMD pathways. *EMBO J.*, **27**, 736–747.
25. Yamashita,A., Ohnishi,T., Kashima,I., Taya,Y. and Ohno,S. (2001) Human SMG-1, a novel phosphatidylinositol 3-kinase-related protein kinase, associates with components of the mRNA surveillance complex and is involved in the regulation of nonsense-mediated mRNA decay. *Genes Dev.*, **15**, 2215–2228.
26. Izumi,N., Yamashita,A., Iwamatsu,A., Kurata,R., Nakamura,H., Saari,B., Hirano,H., Anderson,P. and Ohno,S. (2010) AAA+ proteins RUVBL1 and RUVBL2 coordinate PIKK activity and function in nonsense-mediated mRNA decay. *Sci. Signal.*, **3**, ra27.
27. Hug,N. and Caceres,J.F. (2014) The RNA helicase DHX34 activates NMD by promoting a transition from the surveillance to the decay-inducing complex. *Cell Rep.*, **8**, 1845–1856.
28. Clerici,M., Deniaud,A., Boehm,V., Gehring,N.H., Schaffitzel,C. and Cusack,S. (2014) Structural and functional analysis of the three MIF4G domains of nonsense-mediated decay factor UPF2. *Nucleic Acids Res.*, **42**, 2673–2686.
29. Melero,R., Buchwald,G., Castano,R., Raabe,M., Gil,D., Lazaro,M., Urlaub,H., Conti,E. and Llorca,O. (2012) The cryo-EM structure of the UPF-EJC complex shows UPF1 poised toward the RNA 3′ end. *Nat. Struct. Mol. Biol.*, **19**, 498–505, S491–492.
30. Llorca,O. (2013) Structural insights into nonsense-mediated mRNA decay (NMD) by electron microscopy. *Curr. Opin. Struct. Biol.*, **23**, 161–167.
31. Melero,R., Uchiyama,A., Castano,R., Kataoka,N., Kurosawa,H., Ohno,S., Yamashita,A. and Llorca,O. (2014) Structures of SMG1-UPFs complexes: SMG1 contributes to regulate UPF2-dependent activation of UPF1 in NMD. *Structure*, **22**, 1105–1119.
32. Kadlec,J., Izaurralde,E. and Cusack,S. (2004) The structural basis for the interaction between nonsense-mediated mRNA decay factors UPF2 and UPF3. *Nat. Struct. Mol. Biol.*, **11**, 330–337.
33. Deniaud,A., Karuppasamy,M., Bock,T., Masiulis,S., Huard,K., Garzoni,F., Kerschgens,K., Hentze,M.W., Kulozik,A.E., Beck,M. *et al.* (2015) A network of SMG-8, SMG-9 and SMG-1 C-terminal

insertion domain regulates UPF1 substrate recruitment and phosphorylation. *Nucleic Acids Res.*, **43**, 7600–7611.
34. Buhler,M., Steiner,S., Mohn,F., Paillusson,A. and Muhlemann,O. (2006) EJC-independent degradation of nonsense immunoglobulin-mu mRNA depends on 3′ UTR length. *Nat. Struct. Mol. Biol.*, **13**, 462–464.
35. Eberle,A.B., Stalder,L., Mathys,H., Orozco,R.Z. and Muhlemann,O. (2008) Posttranscriptional gene regulation by spatial rearrangement of the 3′ untranslated region. *PLoS Biol.*, **6**, e92.
36. Chan,W.K., Huang,L., Gudikote,J.P., Chang,Y.F., Imam,J.S., MacLean,J.A. 2nd and Wilkinson,M.F. (2007) An alternative branch of the nonsense-mediated decay pathway. *EMBO J.*, **26**, 1820–1830.
37. Wang,W., Czaplinski,K., Rao,Y. and Peltz,S.W. (2001) The role of Upf proteins in modulating the translation read-through of nonsense-containing transcripts. *EMBO J.*, **20**, 880–890.
38. Nicholson,P., Josi,C., Kurosawa,H., Yamashita,A. and Muhlemann,O. (2014) A novel phosphorylation-independent interaction between SMG6 and UPF1 is essential for human NMD. *Nucleic Acids Res.*, **42**, 9217–9235.
39. Hoshino,S., Imai,M., Mizutani,M., Kikuchi,Y., Hanaoka,F., Ui,M. and Katada,T. (1998) Molecular cloning of a novel member of the eukaryotic polypeptide chain-releasing factors (eRF). Its identification as eRF3 interacting with eRF1. *J. Biol. Chem.*, **273**, 22254–22259.
40. Arias-Palomo,E., Yamashita,A., Fernandez,I.S., Nunez-Ramirez,R., Bamba,Y., Izumi,N., Ohno,S. and Llorca,O. (2011) The nonsense-mediated mRNA decay SMG-1 kinase is regulated by large-scale conformational changes controlled by SMG-8. *Genes Dev.*, **25**, 153–164.
41. Okada-Katsuhata,Y., Yamashita,A., Kutsuzawa,K., Izumi,N., Hirahara,F. and Ohno,S. (2012) N- and C-terminal Upf1 phosphorylations create binding platforms for SMG-6 and SMG-5:SMG-7 during NMD. *Nucleic Acids Res.*, **40**, 1251–1266.
42. Scheres,S.H. (2012) RELION: implementation of a Bayesian approach to cryo-EM structure determination. *J. Struct. Biol.*, **180**, 519–530.
43. Tang,G., Peng,L., Baldwin,P.R., Mann,D.S., Jiang,W., Rees,I. and Ludtke,S.J. (2007) EMAN2: an extensible image processing suite for electron microscopy. *J. Struct. Biol.*, **157**, 38–46.
44. Ludtke,S.J. (2010) 3-D structures of macromolecules using single-particle analysis in EMAN. *Methods Mol. Biol.*, **673**, 157–173.
45. Heymann,J.B. and Belnap,D.M. (2007) Bsoft: image processing and molecular modeling for electron microscopy. *J. Struct. Biol.*, **157**, 3–18.
46. Kataoka,N. and Dreyfuss,G. (2004) A simple whole cell lysate system for in vitro splicing reveals a stepwise assembly of the exon-exon junction complex. *J. Biol. Chem.*, **279**, 7009–7013.
47. Kim,V.N., Kataoka,N. and Dreyfuss,G. (2001) Role of the nonsense-mediated decay factor hUpf3 in the splicing-dependent exon-exon junction complex. *Science*, **293**, 1832–1836.
48. Kong,C., Ito,K., Walsh,M.A., Wada,M., Liu,Y., Kumar,S., Barford,D., Nakamura,Y. and Song,H. (2004) Crystal structure and functional analysis of the eukaryotic class II release factor eRF3 from S. pombe. *Mol. Cell*, **14**, 233–245.
49. Boehm,V., Haberman,N., Ottens,F., Ule,J. and Gehring,N.H. (2014) 3′ UTR length and messenger ribonucleoprotein composition determine endocleavage efficiencies at termination codons. *Cell Rep.*, **9**, 555–568.
50. Bhaskar,V., Roudko,V., Basquin,J., Sharma,K., Urlaub,H., Seraphin,B. and Conti,E. (2013) Structure and RNA-binding properties of the Not1-Not2-Not5 module of the yeast Ccr4-Not complex. *Nat. Struct. Mol. Biol.*, **20**, 1281–1288.
51. Metze,S., Herzog,V.A., Ruepp,M.D. and Muhlemann,O. (2013) Comparison of EJC-enhanced and EJC-independent NMD in human cells reveals two partially redundant degradation pathways. *RNA*, **19**, 1432–1448.
52. Muhlemann,O. (2008) Recognition of nonsense mRNA: towards a unified model. *Biochem. Soc. Trans.*, **36**, 497–501.
53. Singh,G., Rebbapragada,I. and Lykke-Andersen,J. (2008) A competition between stimulators and antagonists of Upf complex recruitment governs human nonsense-mediated mRNA decay. *PLoS Biol.* **6**, e111.
54. Atkin,A.L., Schenkman,L.R., Eastham,M., Dahlseid,J.N., Lelivelt,M.J. and Culbertson,M.R. (1997) Relationship between yeast polyribosomes and Upf proteins required for nonsense mRNA decay. *J. Biol. Chem.*, **272**, 22163–22172.
55. Barbosa,I., Haque,N., Fiorini,F., Barrandon,C., Tomasetto,C., Blanchette,M. and Le Hir,H. (2012) Human CWC22 escorts the helicase eIF4AIII to spliceosomes and promotes exon junction complex assembly. *Nat. Struct. Mol. Biol.*, **19**, 983–990.